THE JOURNAL OF PHYSICAL CHEMISTRY B

Article

pubs.acs.org/JPCB

Ionic Liquids Induced Structural Changes of Bovine Serum Albumin in Aqueous Media: A Detailed Physicochemical and Spectroscopic Study

Tejwant Singh,[‡] Pankaj Bharmoria,[†] Masa-aki Morikawa,[‡] Nobuo Kimizuka,*[,‡] and Arvind Kumar*[,†]

[†]CSIR-Central Salt and Marine Chemicals Research Institute, Council of Scientific & Industrial Research (CSIR), G. B. Marg, Bhavnagar-364002, Gujarat, India

[‡]Department of Chemistry and Biochemistry, Graduate School of Engineering, Centre for Molecular Systems (CMS), Kyushu University, 744-Moto-oka, Nishi-ku, Fukuoka-819-0395, Japan

Supporting Information

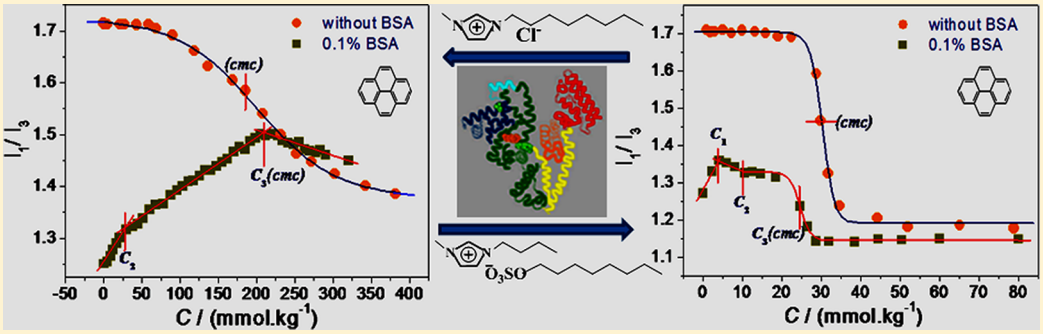

ABSTRACT: Structural changes of a globular protein, bovine serum albumin (BSA), as a consequence of interaction with the surface active ionic liquids (ILs)—3-methyl-1-octylimidazolium chloride, [C_8mim][Cl], and 1-butyl-3-methylimidazolium octylsulfate, [C_4mim][C_8OSO_3]—have been investigated using various physicochemical and spectroscopic techniques such as tensiometry, conductometry, steady-state fluorescence, far-UV circular dichroism spectroscopy (CD), and dynamic light scattering (DLS). The interactional behavior of ILs (monomers and self-assembled structures) toward BSA in different IL concentration regimes at the air/solution interface as well as in the bulk is investigated and discussed depending upon the nature of ions of ILs. CD combined with the steady state fluorescence spectroscopy provided valuable insights into the unfolding of BSA as a consequence of IL binding. The complementary results obtained from the multitechnique approach proved very useful in drawing out the mechanism of interaction between ILs and BSA in different IL concentration regimes.

1. INTRODUCTION

Protein−surfactant interactions have been investigated by various researchers because of their technical application in the field of pharmaceuticals, cosmetics, paints, coatings, and biochemical reactions.[1−5] Moreover, protein−surfactant interactions can provide insights into the effect of surfactants on the native structure of protein in the form of solubilization and denaturing[1,2] or renaturing the protein.[6,7] The globular proteins, in particular, are frequently used as functional ingredients in healthcare and pharmaceutical products because of their ability to catalyze biochemical reactions, to be adsorbed on the surface of some substances, and to bind other molecules and form molecular aggregates.[5] One of the most widely used globular proteins for various technical applications is bovine serum albumin (BSA). BSA is a mammalian albumin made up of 585 amino acid residues with a molecular weight of 66 kDa in a single polypeptide chain[8] and is negatively charged at physiological pH.[9] Various researchers have studied the interactions between BSA and ionic or nonionic surfactants.[10−22] Chakraborty et al. investigated the BSA−SDS interactions using spectrophotometry.[10] The scattering studies of BSA−SDS complexes using SAXS[14] and SANS[15] indicated the change in structure of BSA at higher SDS concentration, while it remained intact at concentrations below the critical aggregation concentration (cac) of surfactant. In their SAXS study, Gelamo et al. showed the higher efficacy of cetyltrimethylammonium chloride (CTAC) over the SDS to unfold the BSA at pH 7.[16] From calorimetric studies, Kelley et al. revealed the stabilization of BSA structure upon monomeric adsorption of SDS at lower concentration and unfolding at higher surfactant concentration, whereas the cationic surfactant dodecyltrimethylammonium bromide (DTAB) caused unfolding at very low concentrations.[18] Chakraborty et al. investigated the physicochemical studies on the interaction of BSA with cationic surfactants alkyltrimethylammonium bromides (ATABs), nonionic pentaethylene glycol mono-*n*-dodecyl

Received: April 14, 2012
Revised: September 3, 2012
Published: September 6, 2012

   dx.doi.org/10.1021/jp303609h | *J. Phys. Chem. B* 2012, 116, 11924−11935

ether ($C_{12}E_5$), and anion surfactant SDS at pH 7 in the presence of 10 mM NaBr and found a surfactant specific interactional process.[19] Turro et al. described the interactional process and modeled the protein−surfactant complexes formed between BSA and SDS using a variety of spectroscopic probe techniques, i.e., fluorescence spectroscopy, electron spin resonance, and nuclear magnetic resonance spectroscopy.[20] Wu et al. studied the interactions between cationic gemini surfactant 1,2-ethane bis(dimethyldodecylammonium bromide) and BSA using far UV-CD spectroscopy and showed the disruption of the helical network of BSA.[21] Li et al. investigated the interactions of BSA with cationic gemini surfactants, alkanediyl-α,ω-bis-(dodecyldimethylammoniumbromide) and single-chain surfactant DTAB at pH 7.0.[22] They concluded that, compared to DTAB, gemini surfactants have much stronger binding ability with BSA and induce the denaturation of BSA at very low concentrations. From these studies, it is inferred that the BSA−surfactant interactions are governed mainly by the nature of surfactant at the pH of physiological interest, and are of much importance from the application as well as academic point of view.

Room temperature ionic liquids (ILs) having amphiphilic character are capturing attention from the scientific community as a novel class of surfactants. The surface activity of these compounds can be easily tailored by the judicious choice of cation or anion. The aggregation behavior of ILs, particularly which are based on imidazolium cation ($[C_n\text{mim}]$) has been intensively studied in recent years by various groups including our research group.[23−40] When compared to the analogous conventional surfactants, the ILs have shown better surface activity.[26,27] Because of their unique physicochemical properties and tailoring nature, ILs can be exploited as superior substitutes to the conventional surfactants in various chemical or biochemical applications. One such field of interest is the use of ILs in conjugation with the proteins for colloidal formulations. Till now, IL−protein interactions were rarely studied. These studies primarily focused on the effect of ILs on protein conformation, aggregation, or oligomerization, stabilization, and dynamics of enzyme/protein,[41−48] and detailed studies on the protein−IL interactions in aqueous solutions are still lacking. In our previous work, we reported the IL−gelatin interactions using various physicochemical techniques.[49] Geng et al. have studied the interaction of a surfactant-like IL, 1-tetradecyl-3-methylimidazolium bromide $[C_{14}\text{mim}][\text{Br}]$ with BSA.[50,51] Recently, Shu et al. have reported the effect of imidazolium based ILs with different anions on BSA.[52] The short chain ILs, incapable of aggregation, have been shown to disrupt the secondary structure of BSA in the studied concentration regime. The binding of ILs with BSA quenched the fluorescence coming from the polypeptide backbone; however, no quenching has been observed for the highly fluorescent amino acid residue, i.e., tryptophan present in domain I and domain II of BSA. The molecular docking studies performed at structurally similar human serum albumin (HSA) showed domain III as the optimum binding site for the IL cation. The authors have limited their study to the very dilute IL concentration regime, the maximum IL concentration investigated being 4.0 mmol L^{-1}, where the IL ions remain in monomeric form. The effectiveness of short chain ILs in their monomeric form to bind specifically to domain III, accompanied by quenching of the fluorescence coming from the polypeptide backbone when excited at 230 nm, and unfolding of BSA by these ILs in the aqueous solutions prompted us to investigate the interactions of BSA with long alkyl chain micelle forming ILs having different characters. Further, no change in fluorescence intensity was observed when the BSA−IL system was excited at 280 nm, where BSA was shown to be highly fluorescent because of strong emission by tryptophan (Trp) and tyrosine (Tyr) residue using 3D fluorescence spectroscopy. We hypothesized that the difference in binding sites depending on the headgroup and alkyl chain length of IL can be probed to get deeper insight into the phenomenon. It would also be interesting to compare the behavior of surface active ILs toward BSA with that of conventional surfactants as well as toward the structurally different protein, gelatin.[49] Therefore, we speculate that the BSA−IL interactions and structural changes induced in BSA as a consequence of interactions of surface active ILs over a wide range of concentration, particularly in the region where self-assembled IL structures are generated, can be of special interest toward understanding of IL−protein colloidal chemistry.

Herein we have investigated in detail the interactions between BSA and amphiphilic ILs: 3-methyl-1-octylimidazolium chloride $[C_8\text{mim}][\text{Cl}]$ and 1-butyl-3-methylimidazolium octylsulfate $[C_4\text{mim}][C_8OSO_3]$ in a wide IL concentration range starting from very dilute (monomeric) to high concentration regimes (above critical micelle concentration, cmc) in aqueous media at pH 7.0 in phosphate buffer medium. On dissolution in water, ILs do not maintain many of the properties of neat ILs; however, the ILs under consideration are surfactant-like ILs[23,25,36] and act as solutions of amphiphiles. The interfacial behavior of ILs in the presence of BSA has been examined using tensiometry. Other techniques such as conductivity, far-UV circular dichroism (CD), fluorescence spectroscopy (extrinsic fluorescence using pyrene as a polarity probe and intrinsic fluorescence of BSA), and dynamic light scattering (DLS) have been used to understand BSA−IL interactions in the bulk, and a model for BSA−IL interactions is proposed. Most of the studies relating to the protein−surfactant interactions as referred above have been carried out either using physical or spectroscopic techniques alone and provide either qualitative or quantitative information. Herein, the multitechnique approach has been found complementary in revealing the interactional behavior, forces involved, structural changes, and nature of complexes in BSA−IL solutions, conspicuously.

2. EXPERIMENTAL SECTION

A. Materials. 3-Methyl-1-octylimidazolium chloride $[C_8\text{mim}][\text{Cl}]$ and 1-butyl-3-methylimidazolium octylsulfate $[C_4\text{mim}][C_8OSO_3]$ with stated purities higher than 98% mass fraction were purchased from Solvent Innovation, Germany. ILs were dried and degassed under vacuum at 60 °C for 2 days to remove moisture. Karl Fischer analysis of the samples indicated that the water content was reduced to less than 0.05%. BSA (M.W. = 66 kDa, purity >98.5%) was purchased from Sigma and was used as received. The solutions of ILs with or without BSA were prepared by weight using an analytical balance with a precision of ±0.0001 g (Denver Instrument APX-200) in phosphate buffer (50 mM, pH 7.0). The buffer solution was prepared in degassed Millipore grade water using AR-grade sodium dihydrogen phosphate and disodium hydrogen phosphate purchased from Merck, India. The stock solution of BSA was stored at 4 °C. The BSA solution was found to be stable at 298.15 K within the

experimental time frame as indicated by a negligible change in CD spectrum with time (Supporting Information, Figure S1).

B. Methods. All measurements were performed in phosphate buffer solution at pH 7.0. BSA solutions were prepared by soaking the BSA powder in buffer for 20 min followed by mild stirring at room temperature. The BSA concentration for the present study was kept at 0.1 wt %. All the experiments were carried out at 298.15 K.

i. Tensiometry. Surface tension measurements were carried out using a Data Physics DCAT II automated tensiometer employing the Wilhelmy plate method. IL was added into the BSA solution by weight and stirred for 3 min for complete solubilization. Prior to measurements, the resultant solutions were kept for 10 min for equilibration. The data was collected in triplicate and was found to be accurate within ±0.1 mN m^{-1}. The temperature of the measurement cell was controlled with a Julabo water thermostat within ±0.1 K.

ii. Conductometry. Electrical conductivities were measured at 298.15 K by a digital conductivity meter (Systronics 308) using a cell of unit cell constant. The temperature of the measurement cell was controlled with a Julabo water thermostat within ±0.1 K. Measurements were performed with an uncertainty of less than 0.5%.

iii. Fluorescence Measurements. Steady-state fluorescence measurements were performed using a Fluorolog (Horiba Jobin Yvon) spectrometer using a quartz cuvette of path length 1 cm. For the fluorescence measurements using pyrene as a polarity probe, the concentration of pyrene used was 2 μM. The emission spectra of pyrene were recorded in the wavelength range 350−500 nm at an excitation wavelength of 334 nm using excitation and emission slit widths of 1 nm. The intrinsic fluorescence of BSA was measured at an excitation wavelength of 280 nm. The maximal values of fluorescence are the average of three measurements. The fluorescence spectra were corrected for the instrumental response.

iv. Far-UV Circular Dichroism Spectroscopy. Far-UV circular dichroism (CD) spectra of 0.1% BSA solutions in buffer solutions of ILs in the wavelength range 200−250 nm were recorded on a Jasco J-815 CD spectrometer at 298.15 K. Experiments were carried out in a 1 mm path length cuvette and were expressed as the average of 10 scans. The spectra were collected at a scan speed of 20 nm per minute. The response time and the bandwidth were 2 s and 0.2 nm, respectively. Samples for recording the spectra were taken in a quartz cuvette which was immediately sealed after sampling to avoid evaporation.

v. Dynamic Light Scattering. Dynamic light scattering measurements (DLS) were performed at 298.15 K on a light scattering apparatus (Spectro Size 300). An appropriate amount of ILs were added by weight to the BSA solution (2 mL) taken in a cylindrical quartz cuvette. The concentration range was varied from very dilute to above the cmc. The temperature of the measurements was controlled with a built-in peltier device with an accuracy of ±0.1 K.

3. RESULTS AND DISCUSSION

A. Micellization of ILs in Buffer at pH 7.0. The tensiometric profiles of aqueous IL solution at pH 7.0 are shown in Figure 1A and B (open symbols). The $[C_4mim][C_8OSO_3]$ is found to be more surface active when compared to $[C_8mim][Cl]$, as evidenced from the lower γ_{cmc} for the former (Table 1). The higher surface activity for $[C_4mim][C_8OSO_3]$ is due to the surface active nature of both the

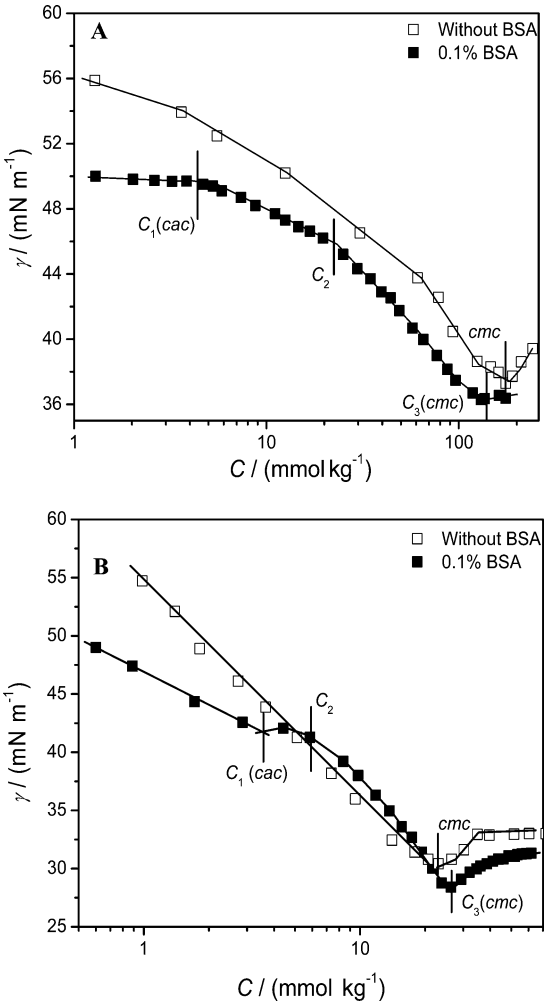

Figure 1. Surface tension (γ) as a function of IL concentration: (A) $[C_8mim][Cl]$ and (B) $[C_4mim][C_8OSO_3]$. Various transitions discussed in the text are marked with vertical lines.

constituent ions of the IL. The pronounced minima near the critical micelle concentration (cmc) in the tensiometric profiles of both of the ILs are observed and attributed to the relative surface excess of water near the imidazolium cation leading to some structural changes as a consequence of anions occupying the interface near the cmc. Similar behavior for aqueous solutions of ILs was also observed by other researchers.[29,30,53] The possibility of impurities producing minima near the cmc cannot be fully ruled out; however, even after the repeated purification of ILs using the procedure reported elsewhere,[54] the minima persist. The cmc, Gibbs' surface excess (Γ_{max}), area of exclusion per monomer (A_{min}), and standard Gibbs free energy of interfacial adsorption (ΔG°_{ad}) (using the Gibbs free energy of micellization ΔG°_{m} deduced from conductivity measurements, Figure 2) are calculated following the standard procedures and equations[55] (see Annexure S1, Supporting Information, for relevant equations and references). The thermodynamic parameters thus obtained are given in Table 1. A comparison of ΔG°_{ad} and ΔG°_{m} shows that interfacial adsorption of ILs is more spontaneous than micelle formation. Figure 2 (open symbols) shows the conductivity profile of the studied ILs. The cmc and degree of ionization, α, deduced from the conductivity data are provided in Table 1. Steady-state fluorescence spectroscopy was used to determine the cmc and

dx.doi.org/10.1021/jp303609h | J. Phys. Chem. B 2012, 116, 11924−11935

Table 1. Critical Micelle Concentration (cmc) from Surface Tension (ST), Conductometry (cond), and Pyrene Probe Fluorescence (flr)[a]

	cmc (mmol kg^{-1})								
	ST	flr	cond	α	ΔG°_{m}	γ_{cmc}	$\Gamma_{max} \times 10^{6}$	A_{min}	ΔG°_{ad}
ILs in Buffer									
[C_8mim][Cl]	170.2	174.2	184.8	0.64	−19.4	37.3	1.24	1.33	−23.1
[C_4mim][C_8OSO_3]	23.0	32.5	29.9	0.34	−30.7	30.5	1.63	1.02	−37.1
ILs in 0.1% BSA Solution									
[C_8mim][Cl]	134.0	208.3	170.1	0.80	−17.3	36.2	1.21	1.37	−29.5
[C_4mim][C_8OSO_3]	26.5	32.4	24.6	0.40	−29.7	29.6	2.01	0.82	−39.9

[a]The degree of counterion binding (α), standard free energy of micellization (ΔG°_{m}), surface tension at cmc (γ_{cmc}), Gibbs' surface excess (Γ_{max}), area of exclusion per monomer (A_{min}), and standard free energy of adsorption (ΔG°_{ad}) at 298.15 K. ΔG°_{m} and ΔG°_{ad} are expressed in kJ mol^{-1}, and γ_{cmc}, Γ_{max}, and A_{min} are expressed in mN m^{-1}, mol m^{-2}, and nm^2 molecule^{-1}, respectively.

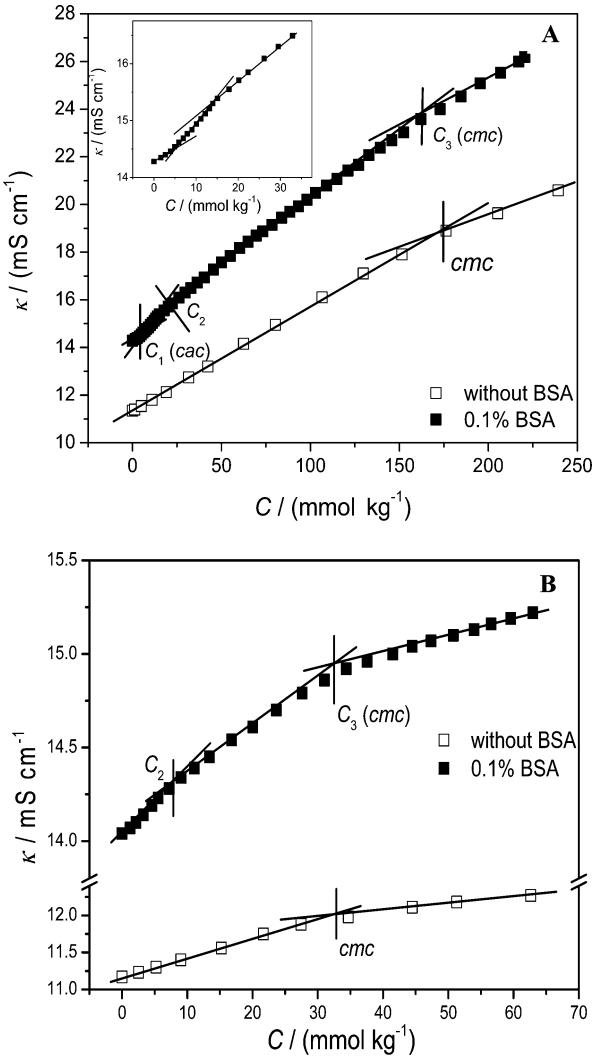

Figure 2. Specific conductance (κ) as a function of IL concentration: (A) [C_8mim][Cl] and (B) [C_4mim][C_8OSO_3], in the absence and presence of 0.1% BSA in buffer. Various transitions discussed in the text are marked. The inset of Figure 1A shows the expanded dilute concentration region.

microenvironment of IL micelles in terms of polarity in the solutions using a pyrene probe. The vibronic bands of the fluorescence spectrum of monomeric pyrene are known to be sensitive to the local polarity. The ratio I_1/I_3 of solubilized pyrene increases on going from nonpolar to polar solvents.[56] The relative intensity of vibronic bands I_1/I_3 of pyrene fluorescence as a function of IL concentration is plotted in Figure 3 (open symbols). The cmc's derived from the midpoint of transition in I_1/I_3 are given in Table 1. The I_1/I_3 values for [C_8mim][Cl] and [C_4mim][C_8OSO_3] were found to be 1.56 and 1.39, respectively, and they suggest a moderate polarity of the cybotactic region as sensed by pyrene in these micelles.

B. BSA−IL Interactions in Buffer at pH 7.0. *i. Tensiometry.* Surface tension measurements were employed to investigate the behavior of BSA in the presence of ILs at the air/solution interface. The tensiometric profiles of [C_8mim][Cl] and [C_4mim][C_8OSO_3] in buffer solutions of 0.1% BSA are shown in Figure 1. The surface tension (γ) of the buffer solution containing BSA is lower than that of pure buffer due to the surface active nature of BSA, indicating the adsorption of some of the BSA at the air/solution interface. Although it is impossible to observe the folding or unfolding of BSA at the interface with the addition of ILs from the changes observed in surface tension, the qualitative information about the BSA−IL interactions can be gained. In the system comprising BSA and [C_8mim][Cl] (Figure 1A, solid symbols), γ initially remains constant up to a particular concentration assigned as the critical aggregation concentration, cac (C_1), indicating the weak interaction of BSA with [C_8mim] and [Cl] ions at the air/solution interface in this concentration regime. The cation [C_8mim] interacts electrostatically with the negatively charged amino acid present at the BSA surface. The interface in this regime is mostly populated by monomeric [C_8mim] supported on polymer chain. After C_1, γ decreases with the increase in [C_8mim][Cl] concentration to reach C_2 from where it follows a comparatively steeper decrease to reach minima at C_3, which is designated as the critical micelle concentration (cmc). The decrease in γ after C_1 indicates stronger BSA−[C_8mim][Cl] interactions. At the studied pH, BSA possesses overall negative charge and the interactions between BSA and [C_8mim][Cl] seem to be electrostatic. However, the role of hydrophobic forces cannot be completely ignored. Following C_1, the electrostatic interaction between positively charged [C_8mim] and the oppositely charged sites of the BSA increases to form surface active electro-neutral BSA−[C_8mim] (monomer) complexes.[57,58] From C_2 onward, the steeper decrease in slope of γ vs IL concentration until C_3 indicates the enrichment of the air/water interface by the monomers which got saturated at C_3. At this stage, the possibility of expulsion of BSA−[C_8mim] (monomer) complexes from the air/solution interface is speculated as the increase in IL concentration may lead to increased hydrophobic interactions between BSA−[C_8mim] (monomer) complexes, thus making the complexes more lipophilic and less surface active.[58] In this region, the BSA−

dx.doi.org/10.1021/jp303609h | J. Phys. Chem. B 2012, 116, 11924−11935

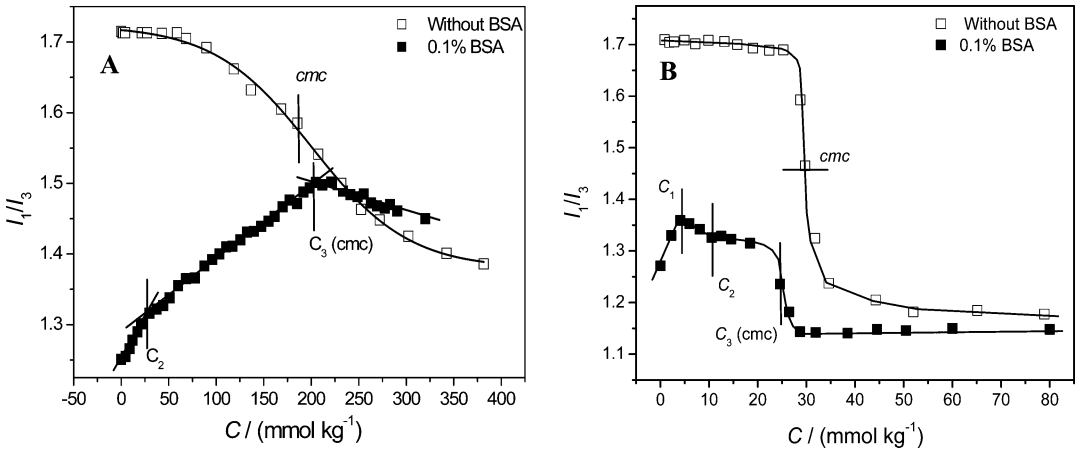

Figure 3. I_1/I_3 in BSA–IL systems as a function of IL concentration: (A) $[C_8mim][Cl]$ and (B) $[C_4mim][C_8OSO_3]$. Various transitions are marked with vertical lines.

Scheme 1. (a) Native BSA, (b) BSA + $[C_8mim][Cl]$, and (c) BSA + $[C_4mim][C_8OSO_3]$[a]

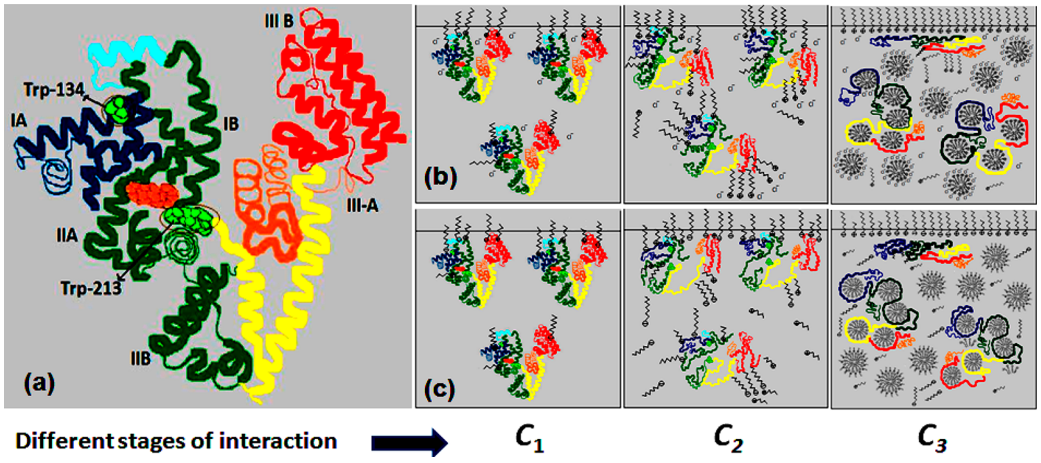

[a] C_1 signifies the cac below which IL ions begins to interact with the BSA at the interface via electrostatic interactions and form BSA–IL (monomer) complexes; C_2 corresponds to BSA–IL (aggregate) complexes driven by both electrostatic and hydrophobic interactions; and C_3 shows the BSA–IL (micelle) complexes and free micelles.

$[C_8mim]$ (monomer) complexes also start to transform to the BSA–$[C_8mim]$ (aggregate) complex in bulk as supported by the conductivity as well as fluorescence measurements. The BSA–$[C_8mim]$ (aggregate) complexes as mentioned above are the complexes formed due to BSA induced aggregation of the surface active moiety $[C_8mim]^+$ on the surface of BSA driven by both electrostatic and hydrophobic interactions.[59] The tensiometric profile for the BSA–ATAB system shows a single break point below the cmc of the surfactant,[19] and thus is simpler than the present BSA–$[C_8mim][Cl]$ tensiometric profile, indicating a different interactional behavior. This can be assigned to the difference in headgroup polarity of the ATABs. The cmc (C_3) of $[C_8mim][Cl]$ in the presence of BSA is lower than that of $[C_8mim][Cl]$ in buffer, indicating the increased interfacial adsorption tendency in the presence of BSA.[19,60] After C_3, the free micelles of $[C_8mim][Cl]$ along with the BSA decorated by $[C_8mim]$ aggregates in the form of BSA–$[C_8mim]$ (aggregate) complex remain in the solution. The interactions of $[C_8mim][Cl]$ with BSA in different concentration regimes are represented in Scheme 1. The C_1, C_2, and C_3 values are reported in Table 2. Thermodynamic parameters, i.e., γ_{cmc}, Γ_{max}, A_{min}, and ΔG°_{ad} (using ΔG°_m from conductivity), calculated for the BSA–$[C_8mim][Cl]$ system are compared in Table 1. A_{min} remains almost constant when compared to that with the BSA free system, indicating a negligible change in the efficacy of $[C_8mim][Cl]$ to populate the interface in the presence of BSA. These results are contrary to that of the gelatin–$[C_8mim][Cl]$ system where the IL showed the decreased ability to populate the interface in the presence of gelatin[49] and may be due to structural differences between the BSA and gelatin. Gelatin, a protein possessing an

Table 2. The Various Transition Concentrations (mmol kg^{-1}) Observed from Various Techniques in BSA–IL Systems at 298.15 K

	ST	cond	Flr (pyrene)	BSA Flr ($\lambda_{emission}$)
		BSA-$[C_8mim][Cl]$		
C_1 (cac)	4.4	4.5		
C_2	15.0	22.0	26.5	17.2
C_3 (cmc)	140.0	170.1	208.3	131.0
		BSA-$[C_4mim][C_8OSO_3]$		
C_1 (cac)	3.5		4.4	
C_2	7.8	7.8	10.4	
C_3 (cmc)	28.4	32.4	24.6	23.5

dx.doi.org/10.1021/jp303609h | J. Phys. Chem. B 2012, 116, 11924–11935

aperiodic structure without any α helical content as compared to BSA, showed strong interactions with $[C_8mim][Cl]$ at the air/solution interface as indicated by an instantaneous decrease in γ with the addition of IL even at very low IL concentration (1 mM) as compared to BSA (4 mM) due to the easy availability of binding sites in the case of gelatin.[61]

$[C_4mim][C_8OSO_3]$ shows different behavior toward BSA at the air/solution interface as compared to $[C_8mim][Cl]$. γ (Figure 1B, solid symbols) decreases linearly with an increase in $[C_4mim][C_8OSO_3]$ concentration up to C_1, thereafter becomes almost constant up to C_2, and then followed by a nonlinear decrease until cmc (C_3). The initial decrease in γ up to the cac (C_1) corresponds to the monomeric adsorption of $[C_8OSO_3]$ at the air/solution interface. At this stage, the positively charged $[C_4mim]$ will be interacting with the peripheral sites of globular BSA, inducing its initial unfolding and exposing both cationic and hydrophobic sites which will be interacting with amphiphilic $[C_8OSO_3]$. At this concentration, both $[C_4mim]$ and $[C_8OSO_3]$ will be forming a BSA−$[C_4mim][C_8OSO_3]$ (monomer) complex due to specific binding to the independent binding sites of BSA, as expressed in Scheme 1. This results in the increased hydrophobicity of the BSA−IL (monomer) complex and leads to preferential adsorption of the complex at the air/solution interface. The special peripheral topology of the globular BSA drives the monomeric interaction of $[C_4mim][C_8OSO_3]$ ions via hydrophobic as well as electrostatic interactions at the investigated pH. In BSA, cationic amino acid residues are peripherally distributed in such a fashion that the hydrophobic interactions between the hydrophobic domains of BSA are reinforced by the ionic interaction between the headgroup and the amino acid residues. Different researchers have reported a similar type of protein−surfactant interactions.[18,19,62] The plateau between C_1 and C_2 corresponds to noncooperative binding of a large number of $[C_4mim][C_8OSO_3]$ ions, preferentially $[C_8OSO_3]$ with the BSA reflecting the increase in surface pressure required for the denaturation of the native BSA structure. With the increase in $[C_4mim][C_8OSO_3]$ concentration, the initially monomerically adsorbed ions lead to an increase in local $[C_4mim][C_8OSO_3]$ concentration in the vicinity of BSA and induce the formation of smaller aggregates to form the BSA−$[C_8OSO_3]$ (aggregate) complex via cooperative binding. Similar observations were made for anionic surfactant SDS where initial specific adsorption of SDS followed by noncooperative binding tailed by cooperative binding to BSA was observed.[19,20] The nonlinear decrease in γ after C_2 up to C_3 is due to interplay between hydrophobic interaction and adsorption of small $[C_8OSO_3]$ aggregates associated with the BSA. Such behavior is also observed in conventional polymer−surfactant systems.[63,64] The saturation of BSA with $[C_8OSO_3]$ aggregates on reaching the C_3 results in the formation of free micelles of $[C_4mim]$-$[C_8OSO_3]$ which remains in solution along with the BSA decorated by $[C_8OSO_3]$ aggregates. The C_1, C_2, and C_3, values are reported in Table 2 and are expressed in Scheme 1. Thermodynamic parameters, i.e., γ_{cmc}, Γ_{max}, A_{min}, and ΔG°_{ad}, calculated for BSA−$[C_4mim][C_8OSO_3]$ systems are compared in Table 1. In the BSA−$[C_4mim][C_8OSO_3]$ system, the A_{min} decreases when compared to that of the BSA free system, indicating the increased efficacy of $[C_4mim]$ and $[C_8OSO_3]$ ions to populate the interface. Interestingly, except the initial interfacially ineffective interaction between gelatin and $[C_4mim][C_8OSO_3]$ ions, the interfacial behavior of $[C_4mim]$-$[C_8OSO_3]$ toward BSA is quite similar to that observed in the presence of gelatin in spite of large structural differences.[49] The difference can be assigned to the presence of a large amount of neutral amino acid residues (glycine and proline) in gelatin where initially it is supposed to have very weak interactions with $[C_4mim]$ and $[C_8OSO_3]$ ions at the air/solution interface as compared to the BSA which has comparatively lower contents of neutral amino acid residues. At higher concentrations, both electrostatic as well as hydrophobic forces seem to play their role in BSA−$[C_4mim][C_8OSO_3]$ interactions. The interplay between BSA and $[C_4mim][C_8OSO_3]$ at the air/solution interface is quite similar to that observed for BSA and SDS, indicating the dominance of $[C_8OSO_3]$ anion as compared to $[C_4mim]$ cation to interact with BSA.[19] The ΔG°_{ad} for the aqueous BSA−$[C_4mim][C_8OSO_3]$ system is higher than the aqueous−$[C_4mim][C_8OSO_3]$ system, indicating preferential adsorption of the ions in at the air/solution interface in the presence of BSA.

ii. Conductometry. The conductometric profiles of $[C_8mim][Cl]$ and $[C_4mim][C_8OSO_3]$ in the presence of 0.1% BSA are shown in Figure 2A and B, respectively. For the BSA−$[C_8mim][Cl]$ system, three distinct transitions which agree well with the C_1, C_2, and C_3 of tensiometry are observed. Initially, the conductivity increases with a lower slope until C_1 fashioned by interaction of $[C_8mim]$ with the oppositely charged surface of BSA, which leads to decreased ionic mobility in the solution as compared to free IL molecules. The changes in the secondary structure of BSA due to unfolding as revealed from CD measurements (section iv) well below the C_1 also demonstrate the specific binding of $[C_8mim]$ to BSA. After C_1, the sharp increase in conductivity until C_2 indicates the increased ionic concentration in the solution. After C_2, a decrease in slope is observed until C_3 following which the conductivity decreases further with a lower slope. The decrease in slope after C_2 indicates the increased BSA−$[C_8mim]$ interactions in the bulk due to increased binding sites on BSA because of the large extent of unfolding of BSA. In this regime, cooperative interactions driven by hydrophobic and electrostatic forces induce the formation of small $[C_8mim][Cl]$ aggregates on the periphery of the BSA. Further, in the same concentration regime, the surface tension measurements also indicate the expulsion of the BSA−$[C_8mim]$ (monomer) complex into the bulk, thereby increasing the effective number of binding sites in the bulk, leading to increased BSA−$[C_8mim][Cl]$ interactions. Similar to that observed from tensiometry, at C_3, the micellization of $[C_8mim][Cl]$ takes place and oppositely charged chloride counterions condense in the stern layer; consequently, a decrease in slope of conductivity has been observed. Similar to the conventional surfactant−polymer systems,[60,65] the degree of counterion ionization (α) was found to be increased in the aqueous BSA−$[C_8mim][Cl]$ system (0.80) when compared to aqueous the $[C_8mim][Cl]$ system (0.64) (Table 1). ΔG°_{m} was found to be slightly lesser in the presence of BSA as compared to the BSA free system, indicating that micellization is slightly more feasible in the latter system.

The conductometric profile of $[C_4mim][C_8OSO_3]$ in the presence of BSA has shown two distinct break points which fairly agrees with C_2 and C_3 observed from the tensiometry (due to less sensitivity of the conductometric technique, C_1 could not be observed). Initially, an increase in the conductivity up to C_2 indicates the increased number of ionic species in the bulk due to specific as well as noncooperative binding of $[C_4mim]$ and $[C_8OSO_3]$ ions to BSA. After C_2, the

dx.doi.org/10.1021/jp303609h | J. Phys. Chem. B 2012, 116, 11924−11935

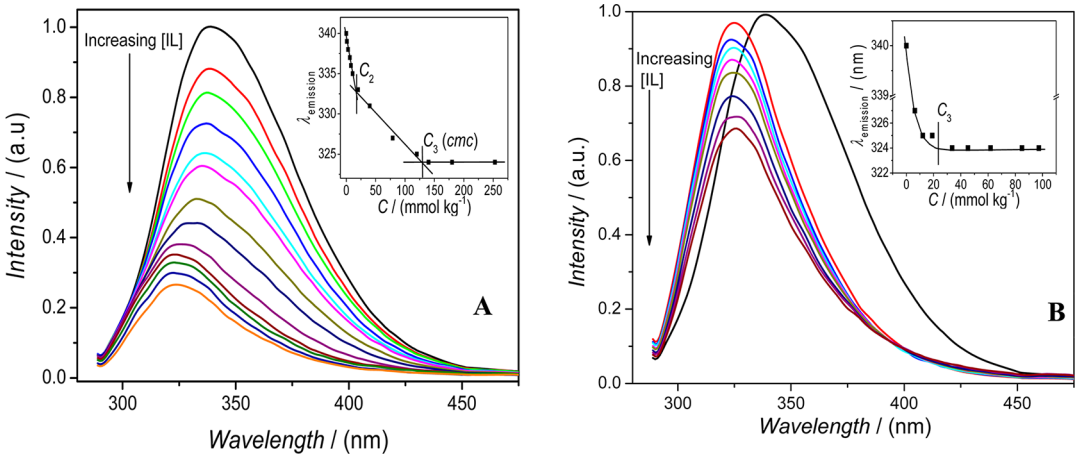

Figure 4. Emission spectra of BSA at an excitation wavelength of 280 nm in the presence of (A) $[C_8mim][Cl]$ and (B) $[C_4mim][C_8OSO_3]$ at various concentrations in buffer solutions. The inset shows the variation of emission wavelength vs IL concentration.

conductivity increases with a slight lower slope, indicating the increased binding of the $[C_4mim]$ and $[C_8OSO_3]$ ions to the BSA which results in the formation of small aggregates onto the surface of BSA via co-operatively driven electrostatic and hydrophobic interactions. After C_3, a decrease in conductivity slope is observed which is due to the formation of free micelle. Similar to the BSA−$[C_8mim][Cl]$ system, the degree of ionization increases and a decrease in the ΔG_m° was observed in the presence of BSA. α, ΔG_m°, and C_1, C_2, and C_3 are given in Tables 1 and 2, respectively. Scheme 1 provides the view of BSA−IL interactions in the bulk.

iii. Fluorimetry. a. Extrinsic Fluorescence. The fluorescence of the polarity probe such as pyrene can be exploited to find the polarity of the cybotactic region of the fluorophore in the protein−IL system.[20,49] Change in the polarity as experienced by the fluorophore provides useful information about the nature of protein−IL interactions. The I_1/I_3 in the BSA solution is much lower than that of buffer solution, indicating that pyrene resides in the hydrophobic domains of the globular BSA. The relative intensity of vibronic bands I_1/I_3 of pyrene fluorescence as a function of IL concentration for BSA−$[C_8mim][Cl]$ and BSA−$[C_4mim][C_8OSO_3]$ is plotted in Figure 3 (solid symbols), respectively. The concentrations corresponding to the observed transitions for both of the ILs are given in Table 2.

With the increase in $[C_8mim][Cl]$ concentration up to C_2, the I_1/I_3 value increases abruptly from the very beginning, indicating enhanced interactions between $[C_8mim][Cl]$ and BSA. In this concentration regime, the unfolding of BSA is observed from CD measurements (section iv) which favors the pyrene to face a more polar environment. The I_1/I_3 value increases with lower slope after C_2 until C_3, indicating less change in polarity and decreased unfolding of BSA at higher $[C_8mim][Cl]$ concentrations. Tensiometric and conductometric measurements indicated existence of the BSA−$[C_8mim]$ (aggregate) complex in this regime. The increase in I_1/I_3 indicates the possibility of partitioning of pyrene in the charged polar network of $[C_8mim]$ ions interacting predominantly via electrostatic and weakly via hydrophobic interactions with BSA accompanied by the unfolding of BSA. After C_3, the I_1/I_3 value decreases with an increase in IL concentration, indicating the decreased polarity of the pyrene cybotactic region due to the incorporation of the pyrene molecules into the IL aggregates decorating BSA and free IL micelles formed at C_3. When compared to gelatin,[49] the behavior of pyrene is quite different. In the very beginning, for the $[C_8mim][Cl]$−gelatin system, I_1/I_3 started decreasing, indicating increased hydrophobic character contrary to the BSA−$[C_8mim][Cl]$ system where we observed the increased hydrophilicity as experienced by pyrene. This might be due to the relatively high hydrophilic environment (I_1/I_3 = 1.69) experienced by pyrene in gelatin solution as compared to BSA (I_1/I_3 = 1.3) in IL free systems, where the partition of pyrene to relatively more hydrophobic gelatin−$[C_8mim]$ (monomer) complexes takes place as compared to the BSA−$[C_8mim][Cl]$ system. The electrostatic interaction between $[C_8mim][Cl]$ and BSA accompanied by unfolding of BSA directs the behavior of pyrene.

With the increase in $[C_4mim][C_8OSO_3]$ concentration up to C_1, the I_1/I_3 value increases sharply, indicating an increase in polarity of the cybotactic region of pyrene due to the unfolding of BSA. However, when compared to the gelatin−$[C_4mim]$-$[C_8OSO_3]$ system, the I_1/I_3 value decreases in this concentration regime. At this stage, it seems that $[C_4mim][C_8OSO_3]$ interacts with BSA via both electrostatic as well as hydrophobic interactions, whereas, in the case of gelatin, the chain contraction on formation of gelatin−$[C_4mim][C_8OSO_3]$ (monomer complex) led to an increase in hydrophobicity. After C_1, a small decrease is observed in the I_1/I_3 value up to C_2 which is due to the incorporation of pyrene in the nonpolar BSA−$[C_4mim][C_8OSO_3]$(aggregate) complex, as evidenced from tensiometric and conductometric measurements. After C_2, the I_1/I_3 decreases very slowly, acquiring almost a plateau showing little change in the polarity with the growth of the BSA−$[C_4mim][C_8OSO_3]$ (aggregate) complex. With the further increase of concentration, I_1/I_3 decreases sharply before reaching an another plateau due to the formation of $[C_4mim][C_8OSO_3]$ micelles. The behavior of I_1/I_3 suggests that, in the BSA−$[C_4mim][C_8OSO_3]$ (aggregate) complex, the pyrene stays in the vicinity of BSA wrapping around the $[C_4mim][C_8OSO_3]$ aggregates until the formation of free micelles of $[C_4mim][C_8OSO_3]$. A comparison of I_1/I_3 behavior of pyrene in the BSA−$[C_8mim][Cl]$ and BSA−$[C_4mim]$-$[C_8OSO_3]$ systems (Figure 3A and B) shows that pyrene feels a more polar environment in the former even above the cac because only $[C_8mim]$ contributes to the hydrophobic environment, whereas the amphiphilic nature of both $[C_4mim]$ and $[C_8OSO_3]$ ions avails a more hydrophobic environment to pyrene in the latter.

dx.doi.org/10.1021/jp303609h | J. Phys. Chem. B 2012, 116, 11924−11935

b. Intrinsic Fluorescence from BSA. The aromatic amino acids tryptophan (Trp), tyrosine (Tyr), and phenylalanine (Phe) act as intrinsic fluorescence probes to study protein conformation, dynamics, and intermolecular interactions. Phe is not excited in most cases, and its quantum yield in proteins is rather low, so the emission from this residue can be ignored.[1,52] The intrinsic fluorescence of the BSA is mainly due to the Trp and Tyr residues as probed by 3D fluorescence spectroscopy.[52] BSA has 2 Trp residues as intrinsic fluorophores, i.e., Trp134 in domain I (subdomain IC) and Trp213 in domain II (subdomain IIA), of its structure and 18 Tyr residues in different domains of BSA. The location of highly fluorescent Trp residues is different; i.e., Trp134 is located on the surface of the molecule and Trp213 is found within a hydrophobic binding pocket of the protein. The Tyr fluorophores are in abundance in subdomain IC of domain I and subdomain IIC of domain II as compared to other subdomains. The intrinsic fluorescence of Trp and Tyr residues can provide very useful information about the BSA−IL interactions[52] similar to that observed for conventional BSA−surfactant systems.[66,67] The changes in the wavelength of the emission maximum (λ_{max}), a parameter sensitive to protein conformation, and fluorescence intensities at 340 nm by excitation at 280 nm where both Trp as well as Tyr residue get excited, can be used to investigate BSA−IL interactions. The possibility of an inner filter effect is ruled out considering the very low absorption of both the excitation wavelength and emission wavelength by the IL (Supporting Information, Figure S2). Figure 4 shows the variation of emission spectra of 0.1% BSA in buffer when excited at 280 nm at different IL concentrations for $[C_8mim][Cl]$ and $[C_4mim][C_8OSO_3]$, respectively. The inset of Figure 4 shows the variation of emission maxima with concentration of respective IL. In the BSA−$[C_8mim][Cl]$ system, a gradual blue shift of the emission maxima is observed with increasing $[C_8mim][Cl]$ concentration, indicating the shift of fluorophores toward a more hydrophobic environment. The fluorophore can get into a more hydrophobic environment by two ways: (1) internalization of fluorophore toward the core of the protein in case the BSA structure gets stabilized; (2) hydrophobic interaction between the nonpolar moieties of ILs and exposed fluorophores, which is possible during the unfolding process. Two breakpoints in the concentration profile (Figure 4A, inset) of λ_{max} are observed, which matches well with C_2 and C_3 as observed by other techniques. The sharp blue shift in λ_{max} up to C_2 is assigned to the change in microenvironment of fluorescent residues by electrostatic and hydrophobic interactions with $[C_8mim]$ at low $[C_8mim][Cl]$ concentration, where the change in secondary structure of BSA is observed even after the monomeric adsorption of $[C_8mim]$ onto BSA. A comparatively lesser blue shift after C_2 until C_3 indicates that there is not much large change in microenvironment of Trp and Tyr residues. In fact, the formation and growth of the BSA−$[C_8mim][Cl]$ (aggregate) complex takes place in this region, as indicated by tensiometric and conductometric measurements. This implies that the formation and growth of the BSA−$[C_8mim][Cl]$ (aggregate) complex occurs via hydrophobic interactions with BSA where the growth of the complex does not alter the microenvironment of Trp and Try residues to a large extent as compared to the low $[C_8mim][Cl]$ concentration regime. After C_3, λ_{max} attains an almost constant value, indicating no observable change in the BSA structure or fluorophore−$[C_8mim][Cl]$ interactions with further addition of $[C_8mim][Cl]$. After this concentration, the growth of the BSA−$[C_8mim]$ (aggregate) complex finishes and free $[C_8mim][Cl]$ micelles form in the solution. Similarly, for the BSA−$[C_4mim][C_8OSO_3]$ system, a blue shift in the emission spectrum is observed, Figure 4B. The inset provides the variation of λ_{max} with $[C_4mim][C_8OSO_3]$ concentration. λ_{max} goes toward blue at low $[C_4mim][C_8OSO_3]$ concentration before attaining a constant value at higher concentrations. No clear break point is observed. In the case of $[C_4mim]$-$[C_8OSO_3]$, both cation as well as anion can interact with the oppositely charged sites of BSA electrostatically and also via hydrophobic means. The blue shift in λ_{max} in the case of the BSA−$[C_4mim][C_8OSO_3]$ system at low concentration seems to be due to stabilization of the native structure of BSA accompanied by a change in the cybotactic region of fluorophores upon interaction with $[C_4mim][C_8OSO_3]$. However, at higher $[C_4mim][C_8OSO_3]$ concentration, the unfolding of the BSA occurs due to the hydrophobic interactions with $[C_4mim]$ and $[C_8OSO_3]$ and causes the blue shift (this is also evidenced by CD measurements).

Further, we expect that the nature of neighboring amino acid residues of both Trp and Tyr residues in terms of their relative polarity and charge will govern the mode and sites of interactions of ILs with BSA. A different number and location of binding sites has been proposed for fatty acids interacting with HSA.[68,69] Moreover, in some studies, the total number of cationic groups on protein are designated as possible binding sites for anionic surfactant, respectively, along with hydrophobic binding.[1] Hence, within the scope of this study, it is very difficult to assign the exact binding sites for ILs to bind with structurally similar BSA in solution. Therefore, in $[C_8mim][Cl]$, the initial binding sites for $[C_8mim]$ cation to BSA are proposed as negatively charged amino acid residues and hydrophobic patches based on the similar phenomenon reported for anionic surfactants where they prefer to bind to positively charged Lys, Arg, and His residues along with hydrophobic binding to hydrophobic regions in the vicinity of cationic sites.[1] The $[C_8mim]$ cation is also supposed to interact with hydrophobic patches in the vicinity of Trp residues, i.e., Trp134 and Trp 213 via hydrophobic interactions, as these residues are surrounded by a positively charged lysine residue. The helical loop in BSA structure located at subdomain IIC seems to be more prone to interact with $[C_8mim]$ cation electrostatically due to the neighboring negatively charged amino acid residues, and the effect is expected to be more reflected due to their comparative large abundance, in fluorescence measurements as compared to Tyr residues present in helical loops of other subdomains, i.e., 1A, 1B, 1C, and 3A. The other possible site of interactions affecting the fluorescence is nonhelical intradomain hinge regions, i.e., the regions 2A−2B, 2C−3A, 3A−3B, and 3B−3C. Contrary to our findings, it has been shown that the presence of short chain ILs with the same cation, i.e., $[C_4mim][Cl]$ and $[C_4mim][NO_3]$, did not affect the fluorescence intensity when the BSA−IL system was excited at 280 nm and the binding site was shown to be located in subdomain 3C based on molecular docking studies performed on HSA.[52] The discrepancy in the results may be accounted for by the higher hydrophobicity of the long alkyl chain in the $[C_8mim]$ cation as compared to the $[C_4mim]$ cation. This further demonstrates that the long chain IL also interacts strongly with highly fluorescent Trp residues. The subdomain 3A has been confirmed as the primary binding site for medium chain fatty acids having chain lengths of carbon atoms of 10 or less.[67] In the BSA−$[C_4mim][C_8OSO_3]$ system,

both the cation and anion may prefer the subdomain 1C and 2C due to the presence of respective oppositely charged amino acid residues in both the subdomains along with other binding sites located in subdomain 3A. Further, similar to SDS, the $[C_8OSO_3]$ anion may interact strongly with Trp 134 located in subdomain 1C which is surrounded by positively charged lysine residues as compared to Trp 213 located in subdomain 2A. Therefore, it is anticipated that the vicinity of Trp 134 is easily influenced by the presence of $[C_8OSO_3]$ anion, which consequently influences the fluorescence behavior of Trp 134 and Tyr residues located in subdomain 1C.

As evident from Figure 4, the addition of ILs decreased the fluorescence intensity of the BSA when excited at 280 nm. The change in fluorescence intensity ratio (I_0/I) of BSA in buffer (I_0) to the BSA solution containing ILs (I) is provided in the Supporting Information, Figure S3. It is observed that the addition of $[C_4mim][C_8OSO_3]$ causes less decrease in fluorescence intensity as compared to $[C_8mim][Cl]$ which indicates their different interactional mechanism with BSA. Similar to SDS,[18] $[C_4mim][C_8OSO_3]$ exerts some stabilization effect on BSA at a very low concentration. It is speculated that the main reason for the decrease in fluorescence intensity is quenching of fluorescence by IL ions similar to that observed in the case of BSA interacting with short chain ILs.[52] It also seems that the BSA unfolding in the present systems does not contribute much to the decreased fluorescence intensity considering the fact that the Stern–Volmer equation for dynamic quenching fitted well to the observed fluorescence data with the intercept of 1. Therefore, the quenching can be interpreted in terms of Stern–Volmer quenching constant using the relation

$$I_0/I = 1 + K_{SV}[Q] = 1 + k_q\tau_0[Q] \quad (1)$$

where I_0 and I stand for the fluorescence intensities in the absence and presence of the quencher (IL), [Q] is the concentration of quencher, $K_{SV} = k_q\tau_0$ is the Stern–Volmer quenching constant (for dynamic quenching), k_q is the bimolecular quenching constant, and τ_0 is the lifetime of the fluorophore in the absence of the quencher. The Stern–Volmer plots for the quenching of BSA fluorescence by $[C_8mim][Cl]$ and $[C_4mim][C_8OSO_3]$ are given in Figure 5 along with the K_{SV} values (0.063 and 0.0045 kg mmol^{-1} for $[C_8mim][Cl]$ and $[C_4mim][C_8OSO_3]$, respectively). The quenching of BSA fluorescence by $[C_8mim][Cl]$ followed the Stern–Volmer plot only in the dilute concentration regime. It deviates at the higher $[C_8mim][Cl]$ concentrations, as can be seen in Figure S3 (see the Supporting Information). The large K_{SV} for $[C_8mim][Cl]$ as compared to $[C_4mim][C_8OSO_3]$ indicates that $[C_8mim][Cl]$ is more efficient in quenching the BSA fluorescence at the studied pH of 7.0. Considering the τ_0 as 10^{-8} s, the k_q comes out to be 6×10^6 and 4×10^5 kg mmol^{-1} s^{-1} for $[C_8mim][Cl]$ and $[C_4mim][C_8OSO_3]$, respectively. This indicates that the quenching of BSA fluorescence is most probably due to the dynamic collision for both of the ILs. k_q is smaller than the largest possible bimolecular quenching constant (1×10^7 mM s^{-1}) in the aqueous media.[52]

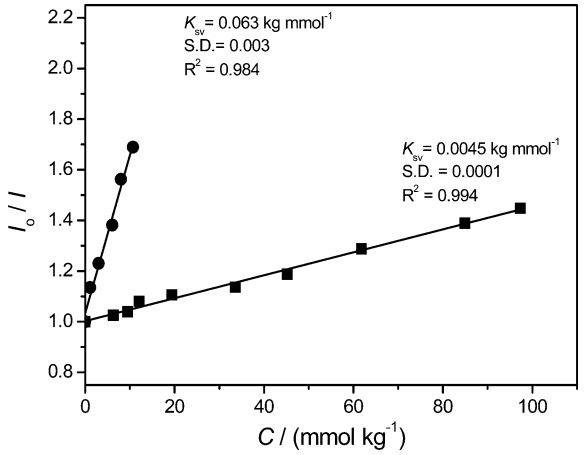

Figure 5. Stern–Volmer plots for quenching of BSA fluorescence by (●) $[C_8mim][Cl]$ and (■) $[C_4mim][C_8OSO_3]$. The fit parameters are provided.

iv. Far-UV CD Spectroscopy. Far-UV CD spectroscopy can be used to probe the changes in secondary structure of the proteins during the denaturation or renaturation process. The CD spectra of the native albumins exhibit two negative bands in the far-UV region at around 208 and 222 nm, characteristic of the α-helical structure.[70] Figure 6 shows CD spectra of 0.1% BSA solution in the far-UV region at different concentrations of $[C_8mim][Cl]$ and $[C_4mim][C_8OSO_3]$. However, the spectra with quite high accuracy could not be measured at high IL concentrations due to high HT voltage and we limited the measurements only to lower IL concentrations. Qualitatively, the magnitude of intensity of the CD spectrum decreases, indicating the decrease in helical content of BSA. Quantitatively, the change in secondary structural content of BSA as a consequence of IL addition has been analyzed using secondary structural analysis software K2D3,[71] and the results are provided as Figure S5 (Supporting Information). In the BSA–$[C_8mim][Cl]$ system, no stabilization of helical structure of BSA is observed; rather, a small decrease in α-helical content from 81 to 77% is observed at very low $[C_8mim][Cl]$ concentration, even well below the cac (C_1). A large decrease in α-helical content is observed just above C_1. It is clear from the CD measurements that BSA unfolds almost completely at or near C_1. Contrary to BSA–$[C_8mim][Cl]$, the stabilization of secondary structure via folding of BSA is revealed by an increase in α-helical content in the BSA–$[C_4mim][C_8OSO_3]$ system at very low $[C_4mim][C_8OSO_3]$ concentration, well below C_1, marked as C_f in Figure S4 (Supporting Information). This initial stabilization leads to enhanced hydrophobicity of fluorescent residues, mainly Trp 134, located in subdomain 1C causing a large blue shift in fluorescent maxima. Following the folding, the unfolding of BSA occurs at the $[C_4mim][C_8OSO_3]$ concentrations above C_f, Figure 5b and Figure S4 (Supporting Information). This unfolding results in increased number of binding sites of BSA for $[C_8OSO_3]$. Here, the quenching of fluorescence takes place without a change in the emission maxima. Similar results were reported by Kelley et al.[18] wherein the initial stabilization of the secondary structure of BSA by SDS at low concentration followed by unfolding was shown. For $[C_8mim][Cl]$ and $[C_4mim][C_8OSO_3]$, the band at 222 nm shifts toward the red by 4 nm above 1.6 and 1.8 mmol kg^{-1}, respectively, Figure S5 (Supporting Information). This red shift in the CD band indicates the presence of hydrogen bonding interactions between the carboxyl or amino groups of different amino acids and protons of imidazolium headgroup/anions. The possibility of hydrogen bonding causing red shift for proteins is reported.[72]

v. Dynamic Light Scattering. Variation in hydrodynamic radii (R_h) of BSA as a consequence of BSA–IL interactions has

dx.doi.org/10.1021/jp303609h | J. Phys. Chem. B 2012, 116, 11924–11935

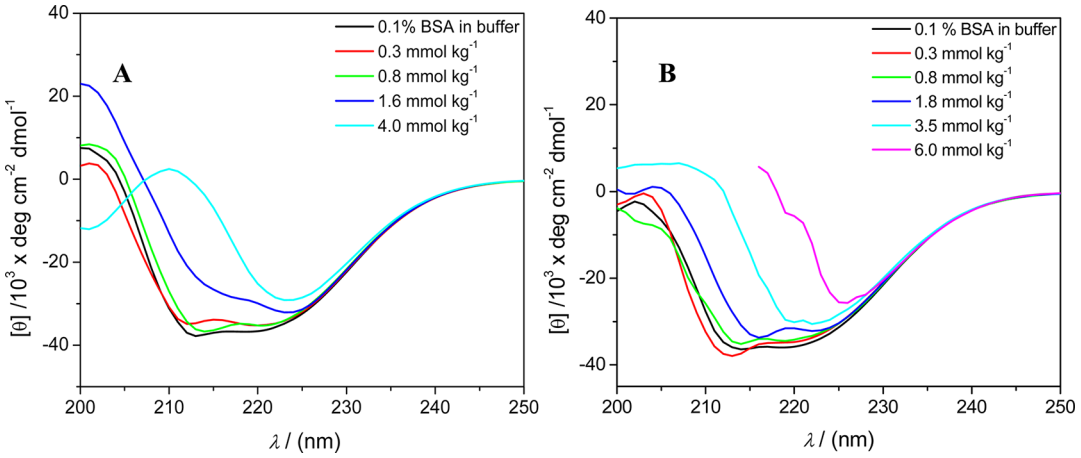

Figure 6. CD spectra of 0.1% BSA in buffer solution in the presence of (A) $[C_8mim][Cl]$ and (B) $[C_4mim][C_8OSO_3]$ at various IL concentrations. Some data has been omitted to avoid crowding for better clarity.

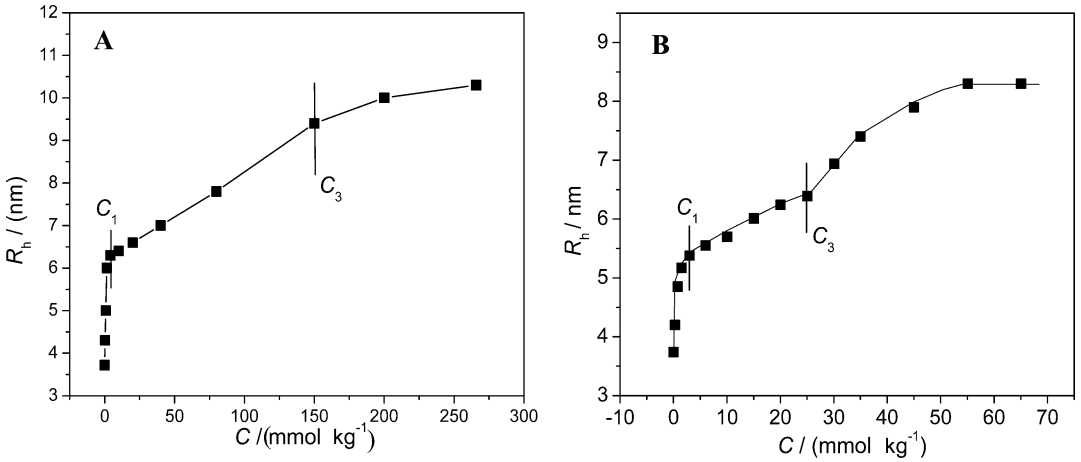

Figure 7. Hydrodynamic radius (R_h) as a function of IL concentration: (A) BSA−$[C_8mim][Cl]$ and (B) BSA−$[C_4mim][C_8OSO_3]$. Various transitions are marked with vertical lines.

been investigated through DLS measurements. The obtained hydrodynamic radii (R_h) and the polydispersity (P_i) are given in Table S1 (Supporting Information). Figure 7 shows the variation of R_h of BSA as a function of IL concentration. For the BSA−$[C_8mim][Cl]$ system, a sharp increase in R_h (approximately 50%) of BSA is observed with the increase in IL concentration until C_1. This increase in R_h is due to monomeric interaction of $[C_8mim]$ cation with the BSA surface accompanied by unfolding of BSA. R_h increases further by ~25% until C_3. The cooperative adsorption of $[C_8mim][Cl]$ on BSA in the form of small aggregates is responsible for this increase in R_h. After C_3, almost no change in the R_h is observed. Similarly, in the BSA−$[C_4mim][C_8OSO_3]$ system, a sharp increase of ~40% in R_h is observed until C_1 which further increases by ~20% up to C_3. Surprisingly, even beyond C_3, the size increases before reaching an almost constant value, indicating that BSA−$[C_4mim][C_8OSO_3]$ (aggregate) complexes are growing in size even after C_3.

CONCLUSIONS

Tensiometric and conductometric profiles revealed that $[C_8mim][Cl]$ interacts with BSA in the bulk prior to interaction at the interface in the dilute concentration regime, whereas a simultaneous interaction at the air/solution interface and in the bulk occurs in the BSA−$[C_4mim][C_8OSO_3]$ system. ΔG°_{ad} and ΔG°_m have been found to be more negative in BSA−$[C_4mim][C_8OSO_3]$ as compared to those in the BSA−$[C_8mim][Cl]$ system, indicating better feasibility of adsorption and micellization of $[C_4mim][C_8OSO_3]$. At low concentration, both $[C_8mim]$ and $[C_4mim]$ interact with BSA electrostatically inducing its unfolding. The magnitude of interaction is stronger for $[C_8mim]$ as compared to $[C_4mim]$, as evident from the higher K_{SV} value (0.063 kg mmol^{-1}) for $[C_8mim][Cl]$ than that of 0.0045 kg mmol^{-1} for $[C_4mim][C_8OSO_3]$. The specific interaction between ILs and BSA persists at lower IL concentration, whereas IL ions bind to BSA cooperatively via electrostatic and hydrophobic interactions at higher IL concentrations. Pyrene fluorescence experiments indicate the dominance of hydrophobic interactions in BSA−$[C_4mim][C_8OSO_3]$ and electrostatic interactions in the BSA−$[C_8mim][Cl]$ system. CD spectroscopy evidenced the presence of hydrogen bonding interactions of the carboxyl or amino groups of different amino acids of BSA with the protons of imidazolium headgroup/anions of ILs and provided useful information about the unfolding of BSA. The multitechnique studies suggest that hydrophobic, electrostatic, and hydrogen bonding interactions are governing the BSA−IL interactions both at the air/solution interface as well as in the bulk, the extent of which depends on the nature of ILs.

dx.doi.org/10.1021/jp303609h | J. Phys. Chem. B 2012, 116, 11924−11935

■ ASSOCIATED CONTENT

Supporting Information

Standard equations for calculating the thermodynamic parameters are given in Annexure S1, Figures S1−S5 contains supporting plots of CD, UV-vis, and fluorescence spectra. Hydrodynamic radii (R_h) and polydispersity index (P) of BSA is provided in Table S1. This material is available free of charge via the Internet at http://pubs.acs.org.

■ AUTHOR INFORMATION

Corresponding Author

*E-mail: mailme_arvind@yahoo.com (A.K.); arvind@csmcri.org (A.K.); n-kimi@mail.cstm.kyushu-u.ac.jp (N.K.). Phone: +91-278-2567039. Fax: +91-278-2567562.

Notes

The authors declare no competing financial interest.

■ ACKNOWLEDGMENTS

P.B. is thankful to Department of Science and Technology (DST), Government of India, for financial support for this work (No. SR/S1/PC-04/2010). T.S. is thankful to JSPS for providing a fellowship. The authors are thankful to the reviewers for very relevant and supportive suggestions which improved the quality of the manuscript.

■ REFERENCES

(1) Ananthapadmanabhan, K. P. In *Interactions of Surfactants with Polymers and Proteins*; Goddard, E. D., Ananthapadmanabhan, K. P., Eds.; CRC Press, Inc: London, U.K., 1993; Chapter 8.
(2) Jones, M. N. *Chem. Soc. Rev.* **1992**, *21*, 127.
(3) Jones, M. N. In *Food Polymers, Gels and Colloids*; Dickenson, E., Ed.; The Royal Society of Chemistry: Cambridge, U.K., 1991; pp 65−80.
(4) McClements, D. J. *Food Emulsions: Principles, Practice and Techniques*, 2nd ed.; CRC Press: Boca Raton, FL, 2004.
(5) Dalgleish, D. G. In *Emulsions and Emulsion Stability*; Sjoblom, J., Ed.; Marcel Dekker: New York, 1996; Chapter 5.
(6) Moriyama, Y.; Takeda, K. *Langmuir* **1999**, *15*, 2003.
(7) Moriyama, Y.; Sato, Y.; Takeda, K. *J. Colloid Interface Sci.* **1993**, *117*, 420.
(8) Giancola, C.; Sena, C. D.; Fessas, D.; Graziano, G.; Barone, G. *Int. J. Biol. Macromol.* **1997**, *20*, 193.
(9) Peters, T. *Advances in Protein Chemistry*; Academic Press: New York, 1985; Vol. *37*, p 161.
(10) Chakraborty, A.; Seth, D.; Setuna, P.; Sarkar, N. *J. Phys. Chem. B* **2006**, *110*, 16607.
(11) Honda, C.; Kamizano, H.; Matsumoto, K.; Endo, K. *J. Colloid Interface Sci.* **2004**, *278*, 310.
(12) Shweitzer, B.; Zanetti, D.; Itri, R. *J. Colloid Interface Sci.* **2004**, *277*, 285.
(13) Xu, Q.; Keiderling, T. A. *Protein Sci.* **2004**, *13*, 2949.
(14) Santos, S. F.; Zanetti, D.; Fischer, H.; Itri, R. *J. Colloid Interface Sci.* **2003**, *262*, 400.
(15) Chen, S. H.; Teixeiria, J. *Phys. Rev. Lett.* **1986**, *57*, 2583.
(16) Gelamo, E. L.; Itri, R.; Alonso, A.; da Silva, J. V.; Tabak, M. J. *Colloid Interface Sci.* **2004**, *277*, 471.
(17) Shinagawa, S.; Sato, M.; Kameyama, K.; Takagi, T. *Langmuir* **1994**, *10*, 1690.
(18) Kelley, D.; McClements, D. J. *Food Hydrocolloids* **2003**, *17*, 73.
(19) Chakraborty, T.; Chakraborty, I.; Moulik, S. P.; Ghosh, S. *Langmuir* **2009**, *25*, 3062.
(20) Turro, N. J.; Lei, X.-G.; Ananthapadmanabhan, K. P.; Aronson, M. *Langmuir* **1995**, *11*, 2525.
(21) Wu, D.; Xu, G.; Sun, Y.; Zhang, H.; Mao, H.; Feng, Y. *Biomacromolecules* **2007**, *8*, 708.
(22) Li, Y.; Wang, X.; Wang, Y. *J. Phys. Chem. B* **2006**, *110*, 8499.
(23) Singh, T.; Kumar, A. *J. Phys. Chem. B* **2008**, *112*, 4079.
(24) Singh, T.; Kumar, A. *Colloids Surf., A* **2008**, *318*, 263.
(25) Singh, T.; Drechsler, M.; Müller, A. H. E.; Mukhopadhyaya, I.; Kumar, A. *Phys. Chem. Chem. Phys.* **2010**, *12*, 11728.
(26) Srinivasa rao, K.; Singh, T.; Trivedi, T. J.; Kumar, A. *J. Phys. Chem. B* **2011**, *115*, 13847.
(27) Dong, B.; Li, N.; Zheng, L.; Yu, L.; Inoue, T. *Langmuir* **2007**, *23*, 4178.
(28) Dong, B.; Zhao, X. Y.; Zheng, L. Q.; Zhang, J.; Li, N.; Inoue, T. *Colloids Surf., A* **2008**, *317*, 666.
(29) Bowers, J.; Butts, P.; Martin, J.; Vergara-Gutierrez, C.; Heenan, K. *Langmuir* **2004**, *20*, 2191.
(30) Goodchild, I.; Collier, L.; Millar, S. L.; Prokeš, I.; Lord, J. C. D.; Butts, C. P.; Bowers, J.; Webster, J. R. P.; Heenan, R. K. *J. Colloid Interface Sci.* **2007**, *307*, 455.
(31) Inoue, T.; Ebina, H.; Dong, B.; Zheng, L. Q. *J. Colloid Interface Sci.* **2007**, *314*, 236.
(32) Dong, B.; Gao, Y.; Su, Y.; Zheng, L.; Xu, J.; Inoue, T. *J. Phys. Chem. B* **2010**, *114*, 340.
(33) Dong, B.; Zhang, J.; Zheng, L. Q.; Wang, S. Q.; Li, X. W.; Inoue, T. *J. Colloid Interface Sci.* **2008**, *319*, 338.
(34) Wang, J.; Wang, H.; Zhang, S.; Zhang, H.; Zhao, Y. *J. Phys. Chem. B* **2007**, *111*, 6181.
(35) Zhao, Y.; Gao, S. J.; Wang, J. J.; Tang, J. M. *J. Phys. Chem. B* **2008**, *112*, 2031.
(36) Miskolczy, Z.; Sebok-Nagy, K.; Biczok, L.; Goektuerk, S. *Chem. Phys. Lett.* **2004**, *400*, 296.
(37) Seth, D.; Sarkar, S.; Sarkar, N. *Langmuir* **2008**, *24*, 7085.
(38) Wang, H. Y.; Wang, J. J.; Zhang, S. B.; Xuan, X. P. *J. Phys. Chem. B* **2008**, *112*, 16682.
(39) Blesic, M.; Lopes, A.; Melo, E.; Petroversuski, Z.; Plechkova, N. V.; Canongia Lopes, J. N.; Seddon, K. R.; Rebelo, L. P. N. *J. Phys. Chem. B* **2008**, *112*, 8645.
(40) Vaghela, N. M.; Sastry, N. V.; Aswal, V. K. *Colloid Polym. Sci.* **2011**, *289*, 309.
(41) Laszlo, J. A.; Compton, D. L. *Biotechnol. Bioeng.* **2001**, *75*, 181.
(42) Eckstein, M.; Sesing, M.; Kragl, U.; Adlercreutz, P. *Biotechnol. Lett.* **2002**, *24*, 867.
(43) Lou, W. Y.; Zong, M. H.; Smith, T. J.; Wu, H.; Wang, J. F. *Green Chem.* **2006**, *8*, 509.
(44) Zhao, H. *J. Mol. Catal. B* **2005**, *37*, 16.
(45) Zhao, H.; Campbell, S. M.; Jackson, L.; Song, Z.; Olubajo, O. *Tetrahedron: Asymmetry* **2006**, *17*, 377.
(46) Constantinescu, D.; Weingärtner, H.; Herrmann, C. *Angew. Chem., Int. Ed.* **2007**, *46*, 8887.
(47) Baker, G. A.; Heller, W. T. *Chem. Eng. J.* **2009**, *147*, 6.
(48) Heller, W. T.; O'Neill, H. M.; Zhang, Q.; Baker, G. A. *J. Phys. Chem. B* **2010**, *114*, 13866.
(49) Singh, T.; Boral, S.; Bohidar, H. B.; Kumar, A. *J. Phys. Chem. B* **2010**, *114*, 8441.
(50) Geng, F.; Zheng, L.; Yu, L.; Li, G.; Tung, C. *Process Biochem.* **2010**, *45*, 306.
(51) Geng, F.; Zheng, L.; Liu, J.; Yu, L.; Tung, C. *Colloid Polym. Sci.* **2009**, *287*, 1253.
(52) Shu, Y.; Liu, M.; Chen, S.; Chen, X.-W.; Wang, J.-H. *J. Phys. Chem. B* **2011**, *115*, 12306.
(53) Sung, J.; Jeon, Y.; Kim, D.; Iwahashi, T.; Iimori, T.; Seki, K.; Ouchi, Y. *Chem. Phys. Lett.* **2005**, *406*, 495.
(54) Singh, T.; Kumar, A. *J. Phys. Chem. B* **2008**, *112*, 4081.
(55) Rosen, M. J. *Surfactant and Interfacial Phenomenon*, 2nd ed.; John Wiley and Sons: New York, 1988.
(56) Kalyanasundaram, K.; Thomas, J. K. *J. Am. Chem. Soc.* **1977**, *99*, 2039.
(57) Miller, R.; Fainerman, V. B.; Makievski, A. V.; Kragel, J.; Grigoriev, D. O.; Kazakov, V. N.; Sinyachenko, O. V. *Adv. Colloid Interface Sci.* **2000**, *86*, 39.
(58) Fainerman, V. B.; Zholob, S. A.; Leser, M. E.; Michel, M.; Miller, R. *J. Phys. Chem. B* **2004**, *108*, 16780.

(59) Jain, N.; Trabelsi, S.; Guillot, S.; McLoughlin, D.; Langevin, D.; Letellier, P.; Turmine, M. *Langmuir* **2004**, *20*, 8496.
(60) Nagarajan, R. *Adv. Colloid Interface Sci.* **1986**, *26*, 205.
(61) Saxena, A.; Antony, T.; Bohidar, H. B. *J. Phys. Chem. B* **1998**, *102*, 5063.
(62) Chen, A.; Wu, D.; Johnson, C. S. *J. Phys. Chem.* **1995**, *99*, 828.
(63) Chakraborty, T.; Chakraborty, I.; Ghosh, S. *Langmuir* **2006**, *22*, 9905.
(64) Griffiths, P. C.; Stilbs, P.; Howe, A. M.; Whitesides, T. H. *Langmuir* **1996**, *12*, 5302.
(65) Cabane, B.; Duplessix, R. J. *J. Phys. (Paris)* **1982**, *43*, 1529.
(66) Gelamo, E. L.; Silva, C. H. T. P.; Imasato, H.; Tabak, M. *Biochim. Biophys. Acta* **2002**, *1594*, 84.
(67) Gelamo, E. L.; Tabak, M. *Spectrochim. Acta, Part A* **2000**, *56*, 2255.
(68) Karush, F.; Sonenberg, M. *J. Am. Chem. Soc.* **1949**, *71*, 1369.
(69) Carter, D. C.; Ho, J. X. *Adv. Protein Chem.* **1994**, *45*, 153.
(70) Takeda, K; Shigeta, M.; Aoki, K. *J. Colloid Interface Sci.* **1987**, *117*, 20.
(71) Louis-Jeune, C.; Andrade-Navarro, M. A.; Perez-Iratxeta, C. *Proteins* **2012**, *80*, 374.
(72) Bloemendal, M.; Johnson, W. C., Jr. In *Physical methods to Characterize Pharmaceutical Proteins*; Herron, J. N., Jiskoot, W., Crommelin, D. J. A., Eds.; Plenum Press: New York, 1995.